Communication

Miniaturization of Omnidirectional Cavity Antennas Using Substrate-Integrated Impedance Surfaces

Yijing He, Yue Li, Liang Zhu, and Pai-Yen Chen

***Abstract*— This communication presents a compact cavity antenna with horizontally polarized omnidirectional radiation pattern. The dimension miniaturization of an omnidirectional resonant cavity is achieved by loading the capacitive substrate-integrated impedance surface (SIIS). Specifically, the SIIS is composed of a row of blind vias that are periodically arranged near the antenna's radiating aperture, effectively providing a shunt capacitance that can be controlled by the insertion depth, period, and diameter of blind vias. The dispersion of the omnidirectional cavity antenna is theoretically studied and the explicit design formula is derived. Our results report that loading the capacitive SIIS can significantly reduce the size of an omnidirectional cavity antenna (52.4%). As a proof of concept, a prototype was fabricated and characterized, with a good agreement between the measurement and simulation results. The results also show that omnidirectional radiation patterns can be maintained well when the operating frequency is tuned, with the realized gain slightly fluctuated between 2.7 and 3.2 dBi. The proposed antenna exhibits potentials in volume-limited omnidirectional wireless communication systems.**

***Index Terms*— Antenna miniaturization, antenna radiation patterns, cavity antennas, reconfigurable antennas, substrate-integrated impedance surfaces (SIISs).**

I. Introduction

Miniaturization is an eternal topic and long-term pursuit in design and development of antennas, and has been extensively investigated in modern wireless communication systems over the past decades [1], [2]. Compact antennas enabling very easy monolithic integration are highly demanded in rapid-deploy, highly compact communication systems, such as satellites, portable hand-held devices, small base stations, and so on [3]–[6]. To date, many approaches have been proposed to achieve miniaturization for the various types of antennas, including slot antennas, cavity antennas, patch antennas, and so on [7]–[12]. For example, antenna miniaturization can be achieved by using high-permittivity substrates, as the size reduction is proportional to $\sqrt{\varepsilon_r}$ [13], [14], where ε_r is the permittivity of dielectric. Shorting plates or pins are also adopted for the same purpose [15]–[17]. By adding a shorting boundary in the center of a patch antenna, the antenna dimension can be reduced by half. Slots-loading technique is another method to miniaturize the antenna dimension. By loading slots on the surface of the planar antenna, the length of current path is increased such that the resonance frequency can be downshifted [18]–[21]. Metamaterial-inspired technique is also utilized to miniaturize the antennas. For instance, metamaterial structures, including split ring resonators (SRRs) or negative-permeability media, can be loaded on the antenna to lower the operating frequency [22]–[27]. There are also other antenna miniaturization techniques, such as fractal apertures or tunable antenna loaded with varactor diodes [28], [29]. Capacitive-loaded technique is applied to novel waveguide topologies such as ridge substrate-integrated waveguides (SIWs) [30], gap waveguides [31], also significantly reducing the size of microwave components such as waveguide antenna array [32].

Omnidirectional antennas play a crucial role in the wireless communication systems, including base stations, wireless local area networks, and portable terminals [33]–[36]. Particularly, horizontally polarized omnidirectional antennas are preferred because they can effectively suppress the diffraction loss, multipath scattering, echoes, and clutters [37]. Alford loop, zeroth-order loop [38], and circular dipole array [39]–[42] are used for horizontally polarized omnidirectional antennas. Another way for horizontally polarized omnidirectional radiation employs an open resonant cavity [43]–[45]. This approach is with the advantages of small cross-sectional area, less complex structure, and no need of additional feeding networks. However, the above open cavity antennas are inherently quarter-wavelength structures, which makes it difficult to be exploited in highly compact wireless communication infrastructures due to the size limitation.

In this work, we propose a simple but effective method to realize miniaturization of horizontally polarized omnidirectional cavity antennas. In our approach, the radiating aperture of the cavity antenna is loaded with the capacitive substrate-integrated impedance surface (SIIS), which consists of an array of periodically positioned blind vias. The explicit formulas for the equivalent surface capacitance of the SIIS as a function of the insertion depth, period, and diameter of vias (see Fig. 1) have been derived in [46]. By controlling the insertion depth, the surface capacitance of the SIIS can be configured to tune the resonance frequency of the omnidirectional cavity antenna without affecting its omnidirectional radiation property. The SIIS-loading technique not only enables miniaturization of the omnidirectional cavity antennas but also provides a widely tunable frequency (from 4.4 to 2.1 GHz) with a low gain variation. In the following, numerical and experimental results for the miniaturized horizontally polarized omnidirectional open cavity antenna are presented.

II. Antenna Design and Implementation

Fig. 1(a)–(c) illustrates the top, lateral, and cross-sectional views of the proposed miniaturized open cavity antenna, as well as the key structural parameters, whose optimal values are summarized in Table I. The antenna consists of a 50 mm × 10 mm × 3 mm

Manuscript received January 18, 2020; revised June 24, 2020; accepted July 15, 2020. Date of publication August 3, 2020; date of current version March 3, 2021. This work was supported in part by the Natural Science Foundation of Beijing Manipulate under Contract 4182029 and in part by the Youth Top Program of Beijing Outstanding Talent Funding Project. *(Corresponding author: Yue Li.)*

Yijing He and Yue Li are with the Department of Electronic Engineering, Tsinghua University, Beijing 100084, China, and also with the Beijing National Research Center for Information Science and Technology, Tsinghua University, Beijing 100084, China (e-mail: lyee@tsinghua.edu.cn).

Liang Zhu and Pai-Yen Chen are with the Department of Electrical and Computer Engineering, University of Illinois at Chicago, Chicago, IL 60607 USA (e-mail: pychen@uic.edu).

Color versions of one or more of the figures in this communication are available online at https://ieeexplore.ieee.org.

Digital Object Identifier 10.1109/TAP.2020.3012493

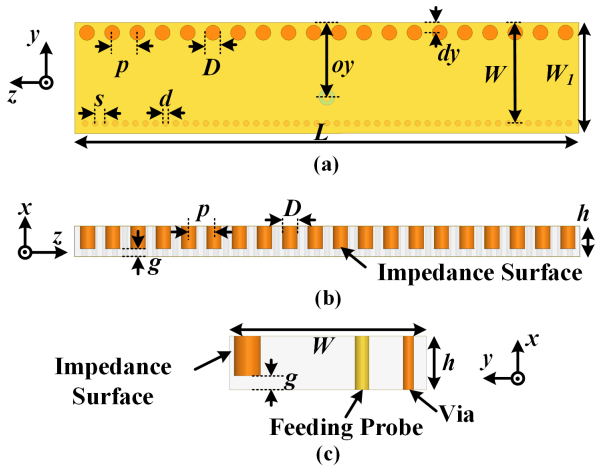

Fig. 1. (a) Top, (b) longitudinal, and (c) cross-sectional views of the proposed SIIS-loaded miniaturized omnidirectional cavity antenna, and the key geometric parameters.

TABLE I

DIMENSIONS OF PROPOSED ANTENNA IN FIG. 2 (UNIT: mm)

p	D	s	d	oy	L	W	W_1	dy	h
2.5	1.5	1.0	0.6	7.4	50.0	10.0	11.0	1.0	3.0

SIW-cavity with its radiating edge being loaded with a capacitive SIIS. This low-profile and low-cost open cavity antenna is based on a single-layer dielectric substrate, F4BM with the relative permittivity $\varepsilon_r = 2.65$, loss tangent $\tan\delta = 0.001$, and thickness $h = 3.0$ mm. The substrate was coated with copper on the top and bottom sides, and metallic through holes were drilled along the side wall of the cavity (see Fig. 1). The SIIS is formed by inserting a row of nonpenetrating blind vias at the antenna's radiating edge. The proposed antenna is excited by a 50 Ω SMA connector, whose inner coaxial probe and outer conductor are soldered to the antenna's top and bottom metallic layers, respectively. The location of the feeding probe on the y-axis was adjusted to achieve impedance matching (see Table I). In this work, commercial software Ansoft High-Frequency Structure Simulator (HFSS) was used to simulate and optimize the proposed antenna.

In this section, we will introduce the concept of SIIS and its applications in miniaturizing an omnidirectional open cavity antenna. The SIIS is composed of a row of blind vias with subwavelength diameter (D), gap (g), and period (p) (see Fig. 1), embedded in an open cavity of thickness h. In this scenario, implanted cut wires and their imaged counterparts mirrored by the top and bottom metal layers of the cavity effectively form a shunt impedance surface. After some mathematical manipulations, the surface impedance of the SIIS can be written as [46]

$$Z_s = \frac{1}{j\omega C_s} \tag{1a}$$

$$C_s = \frac{\varepsilon / p_x p_y}{\{3[\ln(4l/D) - 1]\}/4\pi l^3 - c/(p_x p_y)^{3/2}}[\mathrm{F}] \tag{1b}$$

where l is the length of blind vias ($l = h - g$), c is an empirical fitting parameter, and ε is the permittivity of the dielectric substrate. From (1), it can be found that the surface capacitance C_s can be controlled by the insertion depth (g) and other geometric parameters of the SIIS, including the vias diameter (D) and periodicity

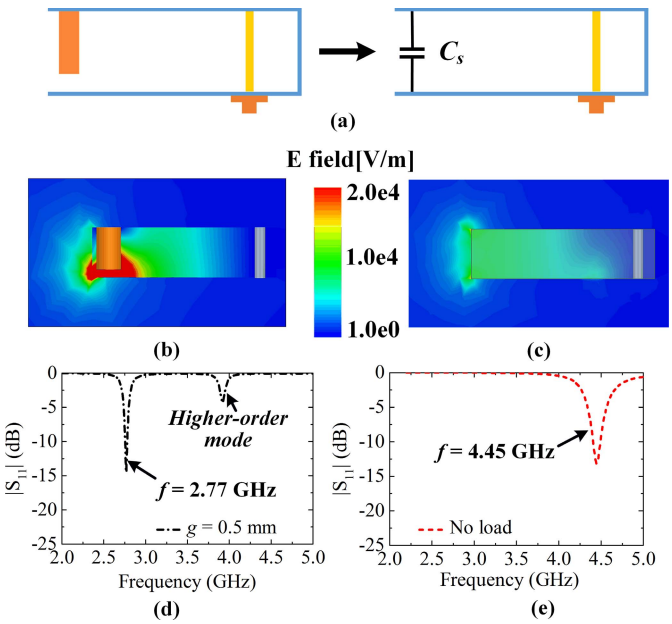

Fig. 2. (a) Open cavity antenna loaded with the capacitive SIIS. Electric field magnitude distributions for the (b) SIIS-loaded open cavity antenna and the (c) conventional open cavity antenna (without SIIS). Reflection coefficient ($|S_{11}|$) versus frequency for (d) SIIS-loaded and (e) conventional open cavity antenna.

($p_x = p$ and $p_y = 2h$). The resonance frequency of the antenna shown in Fig. 1 can be approximately estimated by the cavity model [47], in which the edge consisting of metallic through holes is treated as a perfect electrically conducting (PEC) wall and the three open edges are viewed as perfect magnetically conducting (PMC) walls. If the feed point is placed in the middle of the SIIS-loaded open cavity, the transcendental equation can be derived as

$$\frac{\mathrm{j}\omega\mu_0}{\sqrt{\mathrm{k}^2 - \mathrm{k}_z^2}} \tan\left[\sqrt{\mathrm{k}^2 - \mathrm{k}_z^2}\mathrm{W}\right] + \frac{1}{\mathrm{j}\omega \mathrm{C_s}} = 0 \tag{2}$$

where $\mathrm{k} = \omega\sqrt{\varepsilon\mu_0}$, in which ε and μ_0 are the permittivity and permeability of the dielectric medium inside the cavity, respectively, W is the width of cavity, and the wavenumber along z-direction $\mathrm{k_z} = \mathrm{m}\pi/\mathrm{W}(m = 0, 1, 2, \ldots)$. For the mode with uniformly distributed electric field along the z-direction, $k_z \approx 0$ and, if the antenna has a subwavelength size ($W \ll \lambda_0$), (2) becomes

$$\mathrm{j}\omega(\mu_0 \mathrm{W}) + \frac{1}{\mathrm{j}\omega \mathrm{C_s}} = 0. \tag{3}$$

From (3), it can be observed that the operating frequency of the omnidirectional cavity antenna can be tailored by employing a suitable surface capacitance C_s. Intuitively, when C_s is increased by, for example, increasing the insertion depth of the blind vias [see (1)], the resonance frequency of the SIIS-loaded open cavity antenna will be downshifted. Such properties enable realization of a miniaturized omnidirectional antenna whose operating frequency can be readily altered by varying the height, diameter, and period of blind vias. In addition, we will show in Section III that when the antenna is reconfigured, the impedance matching, radiation efficiency, and omnidirectional characteristic are almost unaffected.

Fig. 2(a) illustrates an SIIS embedded in an open cavity as a shunt capacitive element. Fig. 2(b) and (c) presents the comparison of electric field magnitudes between the SIIS-loaded cavity antenna and the traditional cavity antenna (without the SIIS). From Fig. 2(b), we find that significant electric field enhancement happens in the gap region of the SIIS, implying that geometric/dielectric perturbations in the

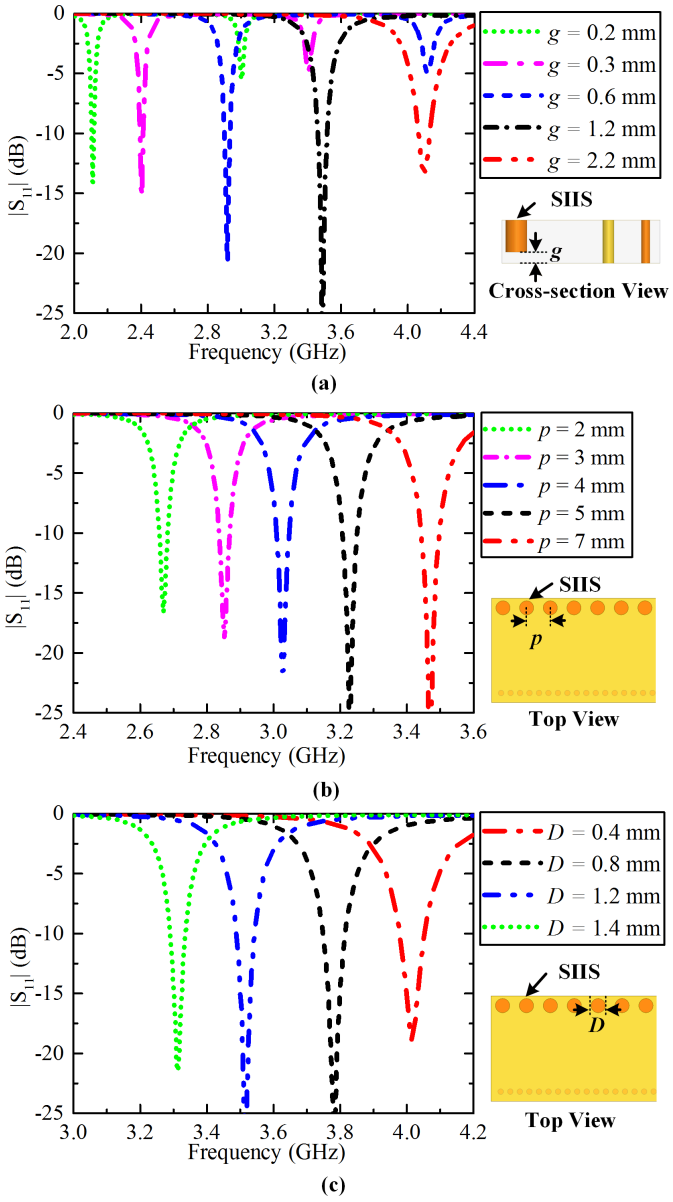

Fig. 3. Simulated reflection coefficients for the proposed miniaturized antenna (a) with g varying from 2.2 to 0.2 [mm], (b) with p changing from 2 to 7 [mm], and (c) with D being swept from 0.4 to 1.4 [mm].

gap area could greatly change the equivalent impedance of the SIIS. Fig. 2(d) and (e) presents the simulated reflection coefficients of the SIIS-loaded and traditional open cavity antenna, respectively. When no SIIS is loaded on the radiating edge, the simulated and calculated resonant frequency is 4.45 and 4.60 GHz, respectively. When the SIIS with $g = 0.5$ mm is loaded on the radiating edge, the simulated operating frequency is considerably downshifted to 2.77 GHz, with the calculated resonant frequency at 2.81 GHz. As a result, loading the SIIS can miniaturize the size of an omnidirectional open cavity antenna. Meanwhile, the calculated and simulated results have a good agreement, verifying the effectiveness of the proposed theoretical formulas for the SIIS-loaded open cavity antenna. According to the perturbation theory [48], [49], strongly localized electric fields found in the gap region of the SIIS allow us to vary the operating frequency over a wide range. The capacitive SIIS also downshifts the higher order resonances of the cavity, as seen in Fig. 2(d).

Fig. 3 reports the simulated reflection coefficients ($|S_{11}|$) for the SIIS-loaded open cavity antenna, of which the structural parameters

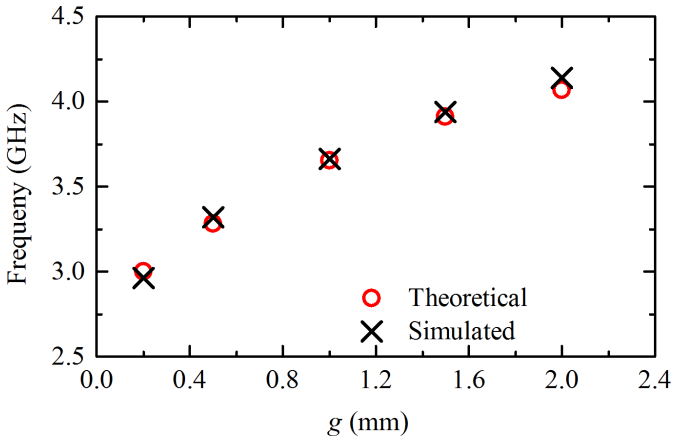

Fig. 4. Theoretical and simulated resonant frequency points of the proposed antenna with gap g swept from 2.0 to 0.2 mm (here, p is fixed to 2.5 mm, $D = 0.6$ mm).

of the blind vias, including gap g, period p, and diameter D, are varied. From Fig. 3(a), it can be seen that when g is swept from 2.2 to 0.2 mm, the operating frequency can be reduced from 4.1 to 2.1 GHz. A large frequency tuning ratio of ~2.1:1 can be achieved through adjustment of the insertion depth of the blind vias. Good impedance matching (< -10 dB) is achieved across the whole tuning range. When operating frequency is reduced, the bandwidth decreases from 70 (1.7%) to 15 MHz (0.66%), due to smaller size and higher quality-factor (Q-factor) of the resonant cavity at low frequencies. This can be understood from Chu–Wheeler's theory. Fig. 3(b) reports reflection coefficients for the SIIS-loaded open cavity antenna with p being varied from 2 to 7 mm; here, g and D are fixed to 0.5 and 1.5 mm. It is seen that increasing the period of blind vias [which reduces the surface capacitance of SIIS; see (1)] upshifts the operating frequency, consistent with (3). Fig. 3(c) is similar to Fig. 3(b), but varying the diameter D of the blind vias; here, g and p are fixed to 0.5 and 2.5 mm, respectively. It can be seen that enlarging the diameter of the blind vias will downshift the operating frequency. These results are consistent with the theoretical predictions and have validated the miniaturization effect of the proposed methodology.

The theoretical resonant frequency can be calculated from (1) and (2). Fig. 4 presents the theoretical and simulated results of the antenna resonance frequency with different gap g. Here, $p = 2.5$ mm, $D = 0.6$ mm, and empirical fitting parameter c is set to be 0.36. As seen, when parameter g is varied from 2.0 to 1.5, 1.0, 0.5, and 0.2 mm, respectively, the simulated resonance frequencies have a good agreement with the theoretical ones, verifying the effectiveness of the derived theoretical formulas. In addition, in this work, length L is not the smallest value the proposed antenna can achieve. We choose length L to be 50 mm to obtain a balanced tradeoff between the antenna size and performances such as bandwidth and realized gain. Further miniaturization of the proposed antenna may be enabled by reducing gap g, and period p, or by increasing diameter D of the SIIS. As an example, a trial maximum miniaturization simulation for the proposed approach is performed here. When $L = 20$ mm, $g = 0.05$ mm, $p = 2.5$ mm, and $D = 2.0$ mm for the proposed antenna, the resonant frequency of the proposed antenna can be reduced to 1.153 GHz, with an electrical size of $0.07\lambda_0 \times 0.04\lambda_0 \times 0.01\lambda_0$ and a miniaturization ratio of 74.0%. At this time, the miniaturized antenna has a fractional operating bandwidth of 0.23% (2.6 MHz), a total efficiency of 53%, a realized gain of -5.8 dBi, and a gain variation of 0.1 dB.

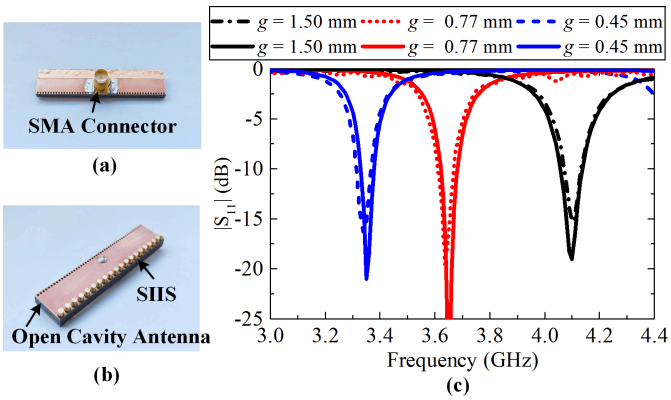

Fig. 5. (a) Bottom view and (b) perspective view of the fabricated prototype of the SIIS-loaded open cavity antenna shown in Fig. 1. (c) Simulated and measured reflection coefficients for the proposed miniaturized antenna with g = 1.50, 0.77, and 0.45 [mm].

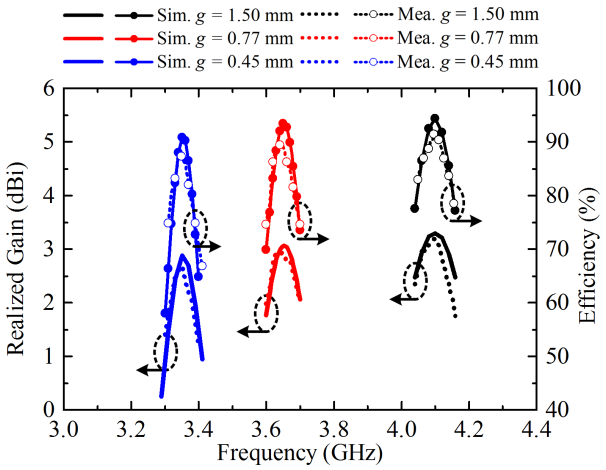

Fig. 6. Simulated and measured realized gain and efficiency of the proposed miniaturized antenna with g = 1.50, 0.77, and 0.45 [mm].

In addition, to make it easier for the readers to understand the proposed method, the design procedures for the dimensions of the cavity are summarized as follows.

1) First, design a regular horizontally polarized omnidirectional open cavity antenna with a dimension of $L \times W \times h$. It is noted that the open cavity antenna operates at $TM_{0,1/2}$ mode (i.e., $k_z = 0$, $k_y = \pi/2W$). L is antenna length, width $W \approx 0.25\lambda_g$, λ_g is the guided wavelength at f_0, h is the substrate thickness.
2) Then, insert the SIIS at the radiating edge of the open cavity with a short distance of s (s is slightly larger than $D/2$). Structural parameters including gap g, period p, and diameter D of the SIIS can be collaboratively designed and optimized to achieve the target frequency f_c. This process can be guided by (1)–(3).

III. Experimental Results

To validate the proposed miniaturized omnidirectional open cavity antenna, a prototype fed by a 50 Ω SMA connector was fabricated and measured, as shown in Fig. 5(a) and (b). As a proof of concept, an open cavity antenna with a row of nonmetallic through holes drilled at the radiating edge was fabricated using standard printed circuit board (PCB) process. An array of identical metallic wires with the same radius and length (5 mm) was inserted into these holes. These blind vias are implemented using identical copper wires made by the precise wire-cutting process. These copper wires are able to remain frozen state due to the enough frictional force brought by the substrate holes. As a principle validation, these copper wires are manually adjusted, and the precision of insertion depth is ensured by an accurate Vernier caliper. A copper foil was used to seal up the metallic bottom part of the cavity. The reflection coefficients were measured using a vector network analyzer (Agilent E5071B), and the far-field radiation patterns were measured in the anechoic chamber. Fig. 5(c) reports the simulated and measured reflection coefficients ($|S_{11}|$) of the proposed miniaturized omnidirectional open cavity antenna. Due to the fabrication error, there exists a small gap of ~0.1 mm between metallic wires and the top metallic surface. This fabrication error has been considered in simulations. The simulated and measured results are in good agreement. From Fig. 5, it is evidently seen that the resonant frequency can be tuned from 4.10, 3.65, to 3.35 GHz, when g is adjusted from 1.5, 0.77, to 0.45 mm. The bandwidth is somewhat reduced from 68 to 60 MHz, when the operating frequency decreases.

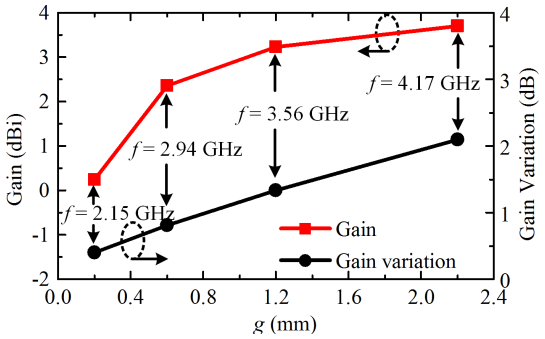

Fig. 7. Simulated gain and gain variation (E-plane) for the proposed miniaturized antenna with different values of g.

Fig. 6 reports the simulated and measured realized gain and total efficiency of the proposed antenna. When g decreases from 1.50 to 0.45 mm, the realized gain is also slightly reduced from 3.2 to 2.7 dBi. As seen, the simulated and measured antenna efficiencies are higher than 92% and 88%, respectively, for all cases. The simulated and measured maximum antenna efficiencies reach 94% and 92%, respectively. The slight differences of less than 4% between the simulated and measured antenna efficiency are within the reasonable range. The high efficiency may be attributed to the nonresonant nature of the SIIS. Fig. 7 illustrates the relationship of the simulated realized gain and the (E-plane) gain variation versus g. When the operating frequency is downshifted by decreasing g from 2.4 to 0.2 mm, the realized gain drops gradually from 3.7 to 0.24 dBi, owing to reduced electrical size of the aperture. The E-plane gain variation also decreases from 2.1 to 0.4 dB. Although adjusting the insertion depth of the blind vias can change the operating frequency, it, however, does not deteriorate the omnidirectional radiation pattern. Fig. 8 reports the co-polarization and cross-polarization radiation patterns on E-plane (xy plane) and H-plane (xz plane) for the proposed antenna operating at 3.35, 3.65, and 4.10 GHz. Both measured and simulated results show that the proposed SIIS-loaded antenna exhibits omnidirectional radiation patterns. The simulated gain variations are less than 1.5 dB and the measured ones are less than 2.6, 3.0, and 3.7 dB for 3.35, 3.65, and 4.10 GHz, respectively. The minor discrepancies between the simulated and experimental results could be due to the errors in testing environments.

It is known that LC circuits or other matching networks are often used to tune the antenna resonant frequency. Actually, the proposed

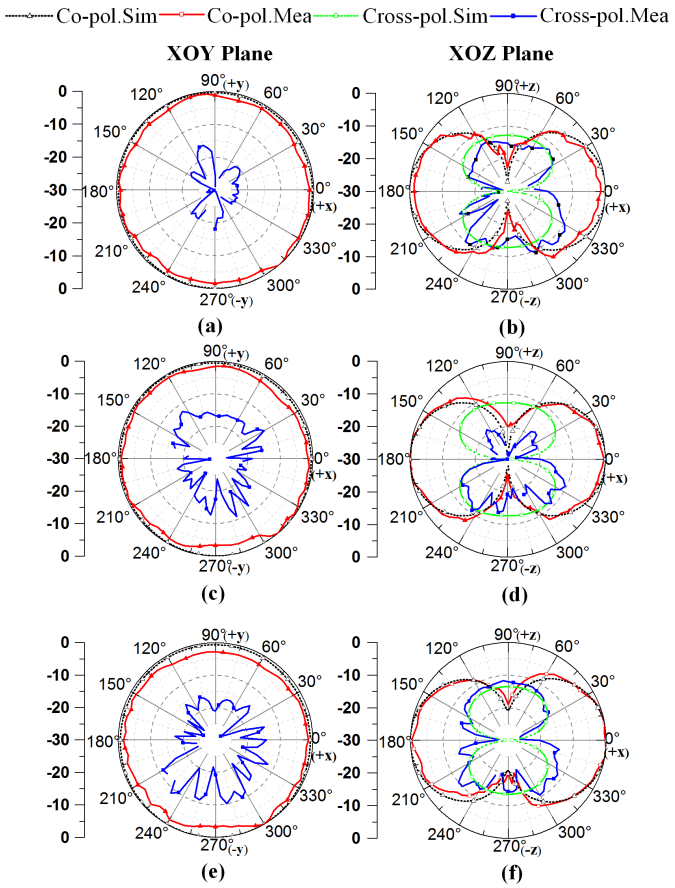

Fig. 8. Simulated and measured normalized radiation patterns of the proposed miniaturized antenna on the *xoy* and *xoz* planes at (a) and (b) 3.35, (c) and (d) 3.65, and (e) and (f) 4.10 GHz.

TABLE II
COMPARISONS BETWEEN PROPOSED DESIGN AND REPORTED WORKS

Ref.	Antenna type	Cross-sectional area(λ_0^2)~(total)	BW (%)	Radiation Efficiency (%)
[39]	Folded dipole	π×0.11×0.11~(0.038)	0.3%	67%
[40]	Cavity	0.088×0.088~(0.008)	3.2%	65.3%
[41]	Cavity	0.35×0.04~(0.014)	2.0%	75%
[42]	Cavity	0.24×0.07~(0.017)	3.2%	N.A.
This work	**Cavity**	**0.12×0.033~(0.004)**	**1.8%**	**88%**

miniaturized antenna also forms an equivalent *LC* circuit. Differently, the equivalent capacitance of SIIS is homogenously distributed on the radiating edge, while *LC* lumped elements or networks are usually loaded on single location. This unique feature brings the proposed antenna an equivalent capacitance with larger value, as a result, a widely tunable performance and a larger miniaturization ratio. In addition, by the virtue of the periodic condition and metasurface theory, the equivalent capacitance of SIIS can be theoretically described using approximately analytical formulas, which have a good agreement with full-wave simulations. On the other hand, the proposed antenna may have more fabrication complexity, which can be improved in the future.

IV. CONCLUSION

In this work, we have proposed an effective approach to realize the miniaturized omnidirectional open cavity antenna. By placing a capacitive SIIS in adjacent to the radiating aperture, the resonance frequency of an open cavity antenna can be tuned over a wide range, whereas its omnidirectional radiation property is well maintained. A prototype has been fabricated and fully characterized to validate the proposed antenna. The measurement results are in agreement with numerical results, showing a realized gain of 2.7–3.2 dBi, an omnidirectional gain variation of 2.6–3.7 dB, a high radiation efficiency more than 88%, and a simulated miniaturization ratio of 52.4%. To highlight the advantages of the proposed antenna over other horizontally polarized omnidirectional antennas, Table II compares the size and performance of the proposed antenna and the existing ones. From this table, it is evident that the proposed antenna has the most compact cross section and a moderately high radiation efficiency (which can be attributed to the nonresonant nature of the SIIS [46]). Therefore, the proposed miniaturized antenna may pave a facile and promising avenue for building highly compact omnidirectional wireless communication and sensing systems.

REFERENCES

[1] A. K. Skrivervik, J.-F. Zurcher, O. Staub, and J. R. Mosig, "PCS antenna design: The challenge of miniaturization," *IEEE Antennas Propag. Mag.*, vol. 43, no. 4, pp. 12–27, Aug. 2001.

[2] J. L. Volakis, C. Chen, M. Lee, B. Kramer, and D. Psychoudakis, "Miniaturization methods for narrowband and ultrawideband antennas," in *Proc. IEEE Int. Workshop Antenna Technol. Small Antennas Novel Metamater.*, Mar. 2005, pp. 119–121.

[3] B. Yuan, Y. Cao, and G. Wang, "A miniaturized printed slot antenna for six-band operation of mobile handsets," *IEEE Antennas Wireless Propag. Lett.*, vol. 10, pp. 854–857, 2011.

[4] S. Chamaani and A. Akbarpour, "Miniaturized dual-band omnidirectional antenna for body area network basestations," *IEEE Antennas Wireless Propag. Lett.*, vol. 14, pp. 1722–1725, 2015.

[5] R. Sammeta and D. S. Filipovic, "Reduced size planar dual-polarized log-periodic antenna for bidirectional high power transmit and receive applications," *IEEE Trans. Antennas Propag.*, vol. 62, no. 11, pp. 5453–5461, Nov. 2014.

[6] T. R. Jones, M. H. Zarifi, and M. Daneshmand, "Miniaturized quarter-mode substrate integrated cavity resonators for humidity sensing," *IEEE Microw. Wireless Compon. Lett.*, vol. 27, no. 7, pp. 612–614, Jul. 2017.

[7] B. Ghosh, S. M. Haque, and D. Mitra, "Miniaturization of slot antennas using slit and strip loading," *IEEE Trans. Antennas Propag.*, vol. 59, no. 10, pp. 3922–3927, Oct. 2011.

[8] Y. Saito and T. Fukusako, "Low-profile and electrically small meander-line antenna using a capacitive feed structure," *IEEE Antennas Wireless Propag. Lett.*, vol. 11, pp. 1281–1284, 2012.

[9] M. Yang, Z. N. Chen, P. Y. Lau, X. Qing, and X. Yin, "Miniaturized patch antenna with grounded strips," *IEEE Trans. Antennas Propag.*, vol. 63, no. 2, pp. 843–848, Feb. 2015.

[10] S. M. Aguilar, M. A. Al-Joumayly, M. J. Burfeindt, N. Behdad, and S. C. Hagness, "Multiband miniaturized patch antennas for a compact, shielded microwave breast imaging array," *IEEE Trans. Antennas Propag.*, vol. 62, no. 3, pp. 1221–1231, Mar. 2014.

[11] Y.-M. Pan, K. W. Leung, and K. Lu, "Compact quasi-isotropic dielectric resonator antenna with small ground plane," *IEEE Trans. Antennas Propag.*, vol. 62, no. 2, pp. 577–585, Feb. 2014.

[12] M. Sun, Y. Ping Zhang, and Y. Lu, "Miniaturization of planar monopole antenna for ultrawideband radios," *IEEE Trans. Antennas Propag.*, vol. 58, no. 7, pp. 2420–2425, Jul. 2010.

[13] T. K. Lo, C.-O. Ho, Y. Hwang, E. K. W. Lam, and B. Lee, "Miniature aperture-coupled microstrip antenna of very high permittivity," *Electron. Lett.*, vol. 33, pp. 9–10, Jan. 1997.

[14] B. Lee and F. J. Harackiewicz, "Miniature microstrip antenna with a partially filled high-permittivity substrate," *IEEE Trans. Antennas Propag.*, vol. 50, no. 8, pp. 1160–1162, Aug. 2002.

[15] C. Y. Chiu, K. M. Shum, and C. H. Chan, "A tunable via-patch loaded PIFA with size reduction," *IEEE Trans. Antennas Propag.*, vol. 55, no. 1, pp. 65–71, Jan. 2007.

[16] S. Choudhury, A. Mohan, and D. Guha, "Wideband quasi-omnidirectional planar inverted F-Antenna for compact wireless systems," *IEEE Antennas Wireless Propag. Lett.*, vol. 17, no. 7, pp. 1305–1308, Jul. 2018.
[17] O. Quevedo-Teruel, E. Pucci, and E. Rajo-Iglesias, "Compact loaded PIFA for multifrequency applications," *IEEE Trans. Antennas Propag.*, vol. 58, no. 3, pp. 656–664, Mar. 2010.
[18] S. Radavaram and M. Pour, "Wideband radiation reconfigurable microstrip patch antenna loaded with two inverted U-Slots," *IEEE Trans. Antennas Propag.*, vol. 67, no. 3, pp. 1501–1508, Mar. 2019.
[19] R. Chair, C.-L. Mak, K.-F. Lee, K.-M. Luk, and A. A. Kishk, "Miniature wide-band half U-slot and half E-shaped patch antennas," *IEEE Trans. Antennas Propag.*, vol. 53, no. 8, pp. 2645–2652, Aug. 2005.
[20] M. W. K. Lee, K. W. Leung, and Y. L. Chow, "Dual polarization slotted miniature wideband patch antenna," *IEEE Trans. Antennas Propag.*, vol. 63, no. 1, pp. 353–357, Jan. 2015.
[21] D. E. Brocker, Z. H. Jiang, M. D. Gregory, and D. H. Werner, "Miniaturized dual-band folded patch antenna with independent band control utilizing an interdigitated slot loading," *IEEE Trans. Antennas Propag.*, vol. 65, no. 1, pp. 380–384, Jan. 2017.
[22] J. Zhu, M. A. Antoniades, and G. V. Eleftheriades, "A compact tri-band monopole antenna with single-cell metamaterial loading," *IEEE Trans. Antennas Propag.*, vol. 58, no. 4, pp. 1031–1038, Apr. 2010.
[23] A. Alù, F. Bilotti, N. Engheta, and L. Vegni, "Subwavelength, compact, resonant patch antennas loaded with metamaterials," *IEEE Trans. Antennas Propag.*, vol. 55, no. 1, pp. 13–25, Jan. 2007.
[24] P.-Y. Chen and A. Alù, "Sub-wavelength elliptical patch antenna loaded with μ-negative metamaterials," *IEEE Trans. Antennas Propag.*, vol. 58, no. 9, pp. 2909–2919, Sep. 2010.
[25] R. O. Ouedraogo, E. J. Rothwell, A. R. Diaz, K. Fuchi, and A. Temme, "Miniaturization of patch antennas using a metamaterial-inspired technique," *IEEE Trans. Antennas Propag.*, vol. 60, no. 5, pp. 2175–2182, May 2012.
[26] Y. Dong, H. Toyao, and T. Itoh, "Design and characterization of miniaturized patch antennas loaded with complementary split-ring resonators," *IEEE Trans. Antennas Propag.*, vol. 60, no. 2, pp. 772–785, Feb. 2012.
[27] S. Jahani, J. Rashed-Mohassel, and M. Shahabadi, "Miniaturization of circular patch antennas using MNG metamaterials," *IEEE Antennas Wireless Propag. Lett.*, vol. 9, pp. 1194–1196, Dec. 2010.
[28] J. P. Gianvittorio and Y. Rahmat-Samii, "Fractal antennas: A novel antenna miniaturization technique, and applications," *IEEE Antennas Propag. Mag.*, vol. 44, no. 1, pp. 20–36, 2002.
[29] M. W. Young, S. Yong, and J. T. Bernhard, "A miniaturized frequency reconfigurable antenna with single bias, dual varactor tuning," *IEEE Trans. Antennas Propag.*, vol. 63, no. 3, pp. 946–951, Mar. 2015.
[30] M. Bozzi, S. A. Winkler, and K. Wu, "Broadband and compact ridge substrate-integrated waveguides," *IET Microw., Antennas Propag.*, vol. 4, no. 11, pp. 1965–1973, 2010.
[31] P.-S. Kildal, A. U. Zaman, E. Rajo-Iglesias, E. Alfonso, and A. Valero-Nogueira, "Design and experimental verification of ridge gap waveguides in bed of nails for parallel plate mode suppression," *IET Microw., Antennas Propag.*, vol. 5, no. 3, pp. 262–270, Mar. 2011.
[32] A. Mallahzadeh and S. Mohammad-Ali-Nezhad, "A low cross-polarization slotted ridged SIW array antenna design with mutual coupling considerations," *IEEE Trans. Antennas Propag.*, vol. 63, no. 10, pp. 4324–4333, Oct. 2015.
[33] C.-C. Lin, L.-C. Kuo, and H.-R. Chuang, "A horizontally polarized omnidirectional printed antenna for WLAN applications," *IEEE Trans. Antennas Propag.*, vol. 54, no. 11, pp. 3551–3556, Nov. 2006.
[34] W. Hong and K. Sarabandi, "Low profile miniaturized planar antenna with omnidirectional vertically polarized radiation," *IEEE Trans. Antennas Propag.*, vol. 56, no. 6, pp. 1533–1540, Jun. 2008.
[35] X. Quan and R. Li, "A broadband dual-polarized omnidirectional antenna for base stations," *IEEE Trans. Antennas Propag.*, vol. 61, no. 2, pp. 943–947, Feb. 2013.
[36] Y. Yu, F. Jolani, and Z. Chen, "A wideband omnidirectional horizontally polarized antenna for 4G LTE applications," *IEEE Antennas Wireless Propag. Lett.*, vol. 12, pp. 686–689, May 2013.
[37] D. Chizhik, J. Ling, and R. A. Valenzuela, "The effect of electric field polarization on indoor propagation," in *Proc. ICUPC 98. IEEE Int. Conf. Universal Pers. Commun. Conf. (ICUPC)*, vol. 1, Oct. 1998, pp. 459–462.
[38] K. Wei, Z. Zhang, Z. Feng, and M. F. Iskander, "A MNG-TL loop antenna array with horizontally polarized omnidirectional patterns," *IEEE Trans. Antennas Propag.*, vol. 60, no. 6, pp. 2702–2710, Jun. 2012.
[39] X. Cai and K. Sarabandi, "A compact broadband horizontally polarized omnidirectional antenna using planar folded dipole elements," *IEEE Trans. Antennas Propag.*, vol. 64, no. 2, pp. 414–422, Feb. 2016.
[40] L. H. Ye, Y. Zhang, X. Y. Zhang, and Q. Xue, "Broadband horizontally polarized omnidirectional antenna array for base-station applications," *IEEE Trans. Antennas Propag.*, vol. 67, no. 4, pp. 2792–2797, Apr. 2019.
[41] H. Liu, Y. Liu, W. Zhang, and S. Gao, "An ultra-wideband horizontally polarized omnidirectional circular connected vivaldi antenna array," *IEEE Trans. Antennas Propag.*, vol. 65, no. 8, pp. 4351–4356, Aug. 2017.
[42] H. Bukhari and K. Sarabandi, "Miniaturized omnidirectional horizontally polarized antenna," *IEEE Trans. Antennas Propag.*, vol. 63, no. 10, pp. 4280–4285, Oct. 2015.
[43] Y. Li, Z. Zhang, J. Zheng, and Z. Feng, "Compact azimuthal omnidirectional dual-polarized antenna using highly isolated colocated slots," *IEEE Trans. Antennas Propag.*, vol. 60, no. 9, pp. 4037–4045, Sep. 2012.
[44] P. Liu, Y. Li, Z. Zhang, and Z. Feng, "Omnidirectional dual-polarized antenna with sabre-like structure," *IEEE Trans. Antennas Propag.*, vol. 65, no. 6, pp. 3221–3225, Jun. 2017.
[45] L. Chang, Y. Li, Z. Zhang, and Z. Feng, "Horizontally polarized omnidirectional antenna array using cascaded cavities," *IEEE Trans. Antennas Propag.*, vol. 64, no. 12, pp. 5454–5459, Dec. 2016.
[46] Y. He, Y. Li, L. Zhu, H. Bagci, D. Erricolo, and P.-Y. Chen, "Waveguide dispersion tailoring by using embedded impedance surfaces," *Phys. Rev. A, Gen. Phys.*, vol. 10, no. 6, Dec. 2018, Art. no. 064024.
[47] C. A. Balanis, *Antenna Theory: Analysis and Design*, 4th ed. Hoboken, NJ, USA: Wiley, 2016, pp. 253–255.
[48] D. M. Pozar, *Microwave Engineering*, 4nd ed. Hoboken, NJ, USA: Wiley, 2012, pp. 306–312.
[49] A. Alù and N. Engheta, "Dielectric sensing in ϵ-near-zero narrow waveguide channels," *Phys. Rev. B, Condens. Matter*, vol. 78, no. 4, pp. 5102-1–5102-5, 2008.